Internal load transfer in an interpenetrating metal/ceramic composite material studied using energy dispersive synchrotron X-ray diffraction

Siddhartha Roy, Jens Gibmeier, Karl Günter Schell, Ethel Claudia Bucharsky, Kay A. Weidenmann, Alexander Wanner, Michael J. Hoffmann

Angaben zur Veröffentlichung / Publication details:

Roy, Siddhartha, Jens Gibmeier, Karl Günter Schell, Ethel Claudia Bucharsky, Kay A. Weidenmann, Alexander Wanner, and Michael J. Hoffmann. 2019. "Internal load transfer in an interpenetrating metal/ceramic composite material studied using energy dispersive synchrotron X-ray diffraction." *Materials Science and Engineering: A* 753: 247–52. https://doi.org/10.1016/j.msea.2019.03.049.

Internal load transfer in an interpenetrating metal/ceramic composite material studied using energy dispersive synchrotron X-ray diffraction

Siddhartha Roy[a,b,*], Jens Gibmeier[a], Karl Günter Schell[c], Ethel Claudia Bucharsky[c], Kay André Weidenmann[a], Alexander Wanner[a], Michael J. Hoffmann[c]

[a] Institute for Applied Materials (IAM-WK), Karlsruhe Institute of Technology, Karlsruhe, 76131, Germany
[b] Department of Metallurgical and Materials Engineering, Indian Institute of Technology, Kharagpur, 721302, India
[c] Institute for Applied Materials – Ceramic Materials and Technologies (IAM-KWT), Karlsruhe Institute of Technology, 76131, Germany

1. Introduction

Among metal matrix composites (MMC) with different phase morphologies, interpenetrating phase composites (IPC) offer good combination of strength, toughness, stiffness, wear resistance and thermal properties along all directions [1–3]. In IPCs the constituent phases are percolating in three dimensions and according to the nomenclature proposed by Newnham et al. [4], a two phase IPC may be classified as a material with 3-3 connectivity. As both the phases are continuous in three dimensions, the designation matrix is no more valid in a strict sense, and hence these composites with one metallic and one ceramic phase as constituents are more commonly referred to as metal/ceramic composites.

The strengthening mechanisms of MMCs can broadly be classified as direct and indirect modes [5]. While direct strengthening occurs by load transfer from the soft, compliant and plastically deforming metallic phase to the stiff and strong ceramic [6]; indirect strengthening is caused by the interactions between dislocations generated at the metal-ceramic interfacial region due to their structural mismatch [7]. MMCs are almost always fabricated at elevated temperatures (either by powder metallurgical or solidification casting route) and due to the significant difference in the thermal expansion coefficients (CTE) of the metallic and the ceramic phases, processing induced thermal residual stresses are generated. As metals generally have higher CTE than the ceramics, the thermal residual stresses are generally tensile in the metallic phase and compressive in the ceramic phase [8,9]. These thermally induced stresses may significantly affect the mechanical properties of MMCs under external loading [10,11]. If a MMC is loaded, when both metallic and ceramic phases are elastic, load shared by both of these phases is not dependent upon the applied stress. At its yield point, the metallic phase starts deforming plastically and its load bearing capacity decreases and the load is transferred to the stiffer and stronger ceramic phase. The extent of load transfer is dependent upon the properties of the two phases, their orientation as well as the strength of the interfacial bond between them. With continuous plastic deformation, the load borne by the ceramic phase continuously increases, until the ceramic fails or a debonding of the interface occurs [12]. The optimum design of MMCs for load bearing applications thrives for

* Corresponding author. Department of Metallurgical and Materials Engineering, Indian Institute of Technology Kharagpur, Kharagpur, 721302, India
E-mail address: siddhartha@metal.iitkgp.ac.in (S. Roy).

maximising the load borne by the ceramic reinforcing phase without damaging it. Hence, thorough understanding of the internal load transfer mechanism is important for any newly developed MMC.

Diffraction based techniques are most commonly employed to study the internal load transfer mechanism in MMCs, as they allow analysing all the crystalline phases of the composite. Elastic lattice strains are measured from the diffraction peak shifts and phase stresses are calculated therefrom. Considering the wealth of information provided by such studies and their importance in understanding the mechanics of MMCs, numerous diffraction based stress analysis studies have been carried out in last about one decade [12–21]. In these previous works, either neutron diffraction or angle dispersive high energy synchrotron X-ray diffraction was employed as both of these techniques allow stress analysis in the bulk of a material. Another diffraction based technique, Energy dispersive synchrotron X-ray diffraction (EDXRD), has also been employed rather successfully for the same purpose [22–28]. EDXRD provides an excellent combination of flux and penetration depth and correspondingly, stress analysis is possible within the bulk of a material using a fairly small gauge volume [29]. Additionally, in EDXRD a white beam is used enabling diffraction analysis over a wide energy range from a multitude of diffraction peaks for all crystalline phases involved. Correspondingly, the calculated average strain is more representative of the real lattice strains in each phase in comparison to analysis based on only one or two diffracting planes; as more commonly employed in neutron diffraction or angle dispersive synchrotron X-ray diffraction.

The current authors recently proposed a simple processing route for fabricating an interpenetrating metal/ceramic composite [30] with easily tailorable phase morphology and phase content. Open porous alumina preforms were fabricated first by burning and sintering a powder mixture of alumina and two different polymer waxes. The porous preforms were then infiltrated with Al12Si melt using inert gas pressure infiltration. Thorough study of the elastic properties was carried out using ultrasound phase spectroscopy, while thermal expansion behaviour was measured by thermal cycling between room temperature and 500 °C. In the present work the mechanism of internal load transfer in one composite sample is studied under external compression by EDXRD. This technique was earlier used very successfully for stress analysis in metal/ceramic composites based on freeze-cast ceramic preforms [23,31] as well as in another interpenetrating composite [24,27]. While the composites based on freeze-cast ceramic preforms had a predominantly lamellar microstructure, the interpenetrating composite had metal rich regions interspersed between ceramic rich regions. The composite studied in this work has a significantly different microstructure and the processing route allows to easily tailor both the phase morphology and the phase contents. Using EDXRD, lattice strains are determined in all three crystalline phases (alumina, silicon and aluminum solid solution) both along and transverse to the loading direction. For each phase, multiple diffraction peaks are analysed for lattice strain determination and correspondingly the extent of interplanar anisotropy can also be investigated. Phase stresses as well as the stress concentration factors are simultaneously calculated from the measured lattice strains using standard elasticity relations. This way a thorough study of internal load transfer mechanism in this interpenetrating metal/ceramic composite has been carried out.

2. Experimental procedure

2.1. Specimen material

A very brief description of the studied IPC is provided here and for a thorough description of the microstructure of both the preforms and the composite we refer to Ref. [30]. Porous alumina preforms were first fabricated by burning and sintering a cold pressed green body formed from a mixture of alumina powder and two different polymer waxes. One of the polymer waxes was coarse grained and the other one was much finer and they were mixed in 1:1 ratio in the initial powder mixture. The alumina:total wax mixture ratios were varied to fabricate preforms having open porosities in the range of 55–65 vol%. The sintered open porous preforms were subsequently infiltrated with molten Al12Si alloy using inert argon gas pressure. To perform the melt infiltration, the porous preforms along with billets of Al12Si were placed inside a pressure chamber. The chamber was initially evacuated to remove all air from the porous preforms and subsequently the temperature inside the chamber was raised to 750 °C. Finally pressure using argon gas was applied on the molten metal to infiltrate the porous preforms to form the IPC.

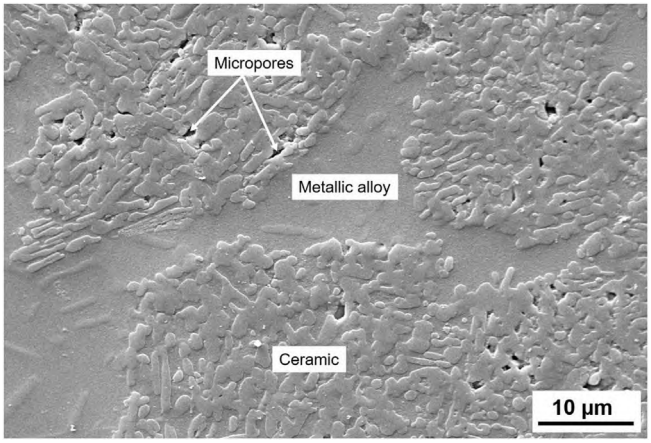

Fig. 1. Typical SEM image of the studied interpenetrating Al12Si/alumina composite.

A typical SEM image of the studied IPC is shown in Fig. 1. Regions of the metallic alloy as well as the ceramic rich regions are shown marked in this micrograph. The solubility of aluminum in silicon is almost negligible and correspondingly the metallic alloy consists of needle shaped pure silicon particles distributed within aluminum solid solution [32]. Some micropores are also marked and they are typically found within the ceramic rich regions due to lack of complete infiltration within the densely packed ceramic rich regions. Presence of such residual microporosities within ceramic rich regions in MMCs have also been reported by earlier studies [24,33]. Density of the studied IPC samples was measured following Archimedes principle by immersing in distilled water.

2.2. In-situ energy dispersive synchrotron x-ray diffraction (EDXRD) experiment

The experiment was carried out at the Materials Science Beamline EDDI at the BESSY synchrotron radiation source at Berlin, Germany. Thorough description of the beamline components can be found in Ref. [34]. Uniaxial compression test of one IPC sample was carried out in-situ in a miniature tensile compression module manufactured by Kammrath & Weiss GmbH (Dortmund, Germany). An image of the mechanical test module mounted on the diffraction table is provided in Ref. [23]. The module was mounted on the motorized table of the diffractometer unit which consisted of a θ-θ diffractometer, a five axis sample positioning unit as well as a detector arm with two slit systems to define the diffracted beam. For the current experiment the primary beam was masked by a cross slit system with an opening of 1 mm × 1 mm; while the slits in the path of the diffracted beam had dimensions of 0.06 mm × 8 mm. The sample used for in-situ compression test had dimensions of 2.66 mm × 2.65 mm × 2.56 mm and 20 µm thick aluminum foil was used between the sample and the hardened punches to reduce frictional effect. For the diffraction experiments a constant scattering angle of $2\theta = 10.23^{\circ}$ was chosen as it provides both, good energy separation and a sufficient peak intensity for analysis. Density of the sample was measured from its mass and dimensions and

it corresponded to a ceramic content of 42 vol% assuming no porosity. A preload of −43 N (corresponding to a compressive stress of about 6 MPa) was first applied to ensure the sample did not displace during subsequent experiment. Lattice spacing in all indexed diffraction planes of the three phases with only this preload was measured and this was used as the reference value for subsequent lattice strain calculation. Correspondingly, processing induced thermal residual stresses were not measured and only the change in lattice spacing caused solely by the external compressive stress has been analysed. Compression test was carried out at a constant crosshead velocity of 2 μm s^{-1}, corresponding to a nominal strain rate of 10^{-3} s^{-1}. Compressive load on the sample was increased stepwise and at each step the test was stopped and diffraction measurements were carried out following the $sin^2\psi$ method [35] of stress analysis by stepwise tilting the test setup between $\psi = 0^\circ$ and 89.9°. Following compressive stress steps (all in MPa) were employed 6 → 27 → 52 → 76 → 105 → 145 → 187 → 228 → 274 → 316 → 349 → 396 → 430. Previous stress analysis on Al12Si/alumina interpenetrating composites showed that plastic deformation of the metallic phase initiates in the range of 80 MPa compressive stress [23,27]. Correspondingly, the steps for diffraction based stress analysis were maintained at around 25 MPa until about 100 MPa applied compressive stresses and subsequently the gap between each step was increased to approximately 40 MPa. After each load application and before each diffraction measurement sufficient waiting time was maintained to minimize the effects of stress relaxation in the sample during the diffraction measurement itself. Individual diffraction peaks were fitted by a Pseudo-Voigt function to determine the peak positions. Lattice strains were determined from the calculated lattice plane spacings) according to the following relation

$$\varepsilon = \frac{d^{hkl} - d_0^{hkl}}{d_0^{hkl}} \quad (1)$$

where d_0^{hkl} corresponds to the lattice plane spacing in the initial state (with the applied preload of −43 N) and d_{hkl} corresponds to the corresponding lattice plane spacing at different applied stresses.

3. Results and discussions

Fig. 2 shows typical EDXRD diffractogram of the studied IPC sample. The indexed diffraction planes employed for lattice strain analysis are marked in the figure. 7 diffraction planes of alumina, 4 diffraction planes of aluminum solid solution and 3 diffraction planes for pure silicon were indexed. At each applied load step and for all diffracting planes of the three crystalline phases, d-spacing vs. $sin^2\psi$

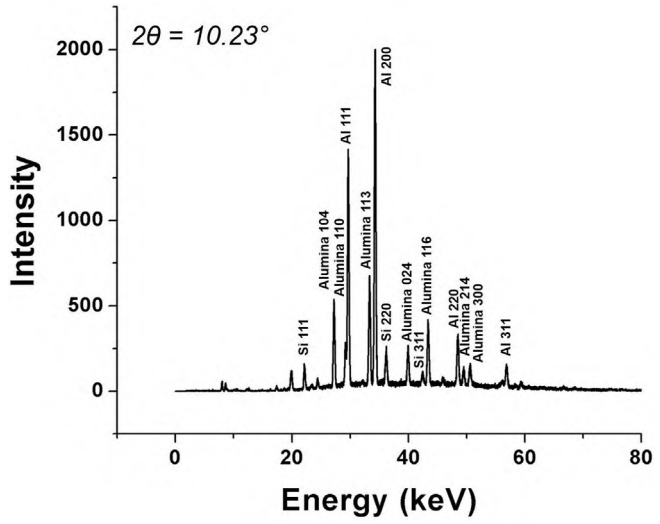

Fig. 2. Typical EDXRD diffractogram obtained for the IPC sample studied.

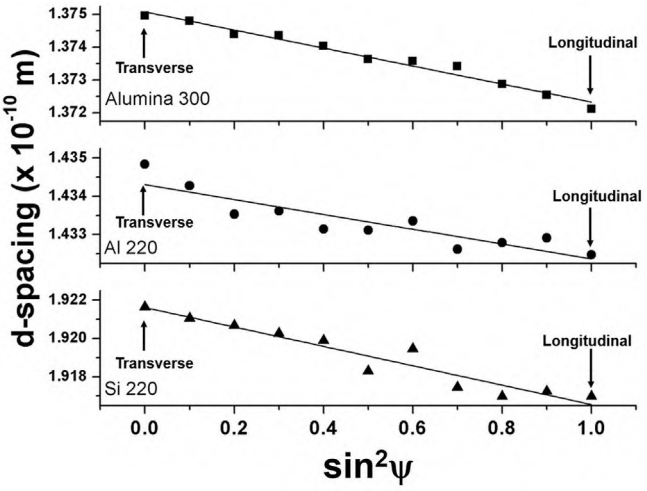

Fig. 3. d-spacing vs. $sin^2\psi$ plots for {300} planes of alumina, {220} planes of aluminum solid solution and {220} planes of silicon at an applied compressive stress of −274 MPa.

plots were made at eleven different ψ-tilts between 0° and 89.9°. Subsequently, best fit straight lines were calculated for each d-spacing vs. $sin^2\psi$ plot. Determination of the longitudinal and transverse lattice spacings from the best fit straight lines drawn based on multiple ψ-tilts ensured a much better statistical confidence in comparison to measurements carried out at only two extreme tilts of 0° and 89.9°. At $\psi = 89.9^\circ$ the scattering vector was almost parallel to the loading direction and at $\psi = 0^\circ$ the scattering vector was nearly transverse to the loading direction. At each applied stress step and for all analysed diffraction planes, the lattice plane spacings along and transverse to the loading direction were finally determined from the best fit straight lines. Fig. 3 shows representative d-spacing vs. $sin^2\psi$ plots for {300} planes of alumina, {220} planes of Al solid solution and {220} planes of silicon. Similar plots were also obtained for other diffraction planes.

Fig. 4 shows the evolution of lattice microstrain along the loading direction (hereafter named as longitudinal lattice strain) as a function of the applied compressive stress in all three crystalline phases of the composite material. The plots a-c in this figure show the evolution of longitudinal microstrain in all indexed diffraction planes of alumina, aluminum and silicon, respectively. For each phase the continuum mechanics average lattice microstrain was calculated according to the methodology proposed by Daymond [36], considering the multiplicity factor and diffraction elastic constants of each diffraction plane and assuming absence of any texture (texture factor taken as unity). This continuum mechanics average microstrain for all three phases is also shown in each plot as bold lines and additionally they are plotted separately in Fig. 4d against the applied compressive stress for the sake of clarity. The error bars on the lines for average microstrains of each phase correspond to the standard deviation of the lattice strains measured by all indexed diffractions planes of that phase and they are a measure of the interplanar anisotropy.

Fig. 4 shows that at low applied compressive stresses until about 100 MPa, the longitudinal lattice strain in all three phases increase almost linearly. At this stage, all phases of the composite are undergoing only elastic deformation. At higher applied stresses however the lattice microstrain in aluminum solid solution increases at a slower rate, suggesting a decrease in the load carrying capacity of aluminum solid solution. Corresponding to the downward trend of the longitudinal strain in aluminum solid solution due to its plastic deformation, the curve for the alumina phase should show an upward trend as load is being transferred from aluminum solid solution to this phase (as was reported in Ref. [27]). However, no such clearly discernible upward trend is observed in alumina and the slope for the curve for alumina

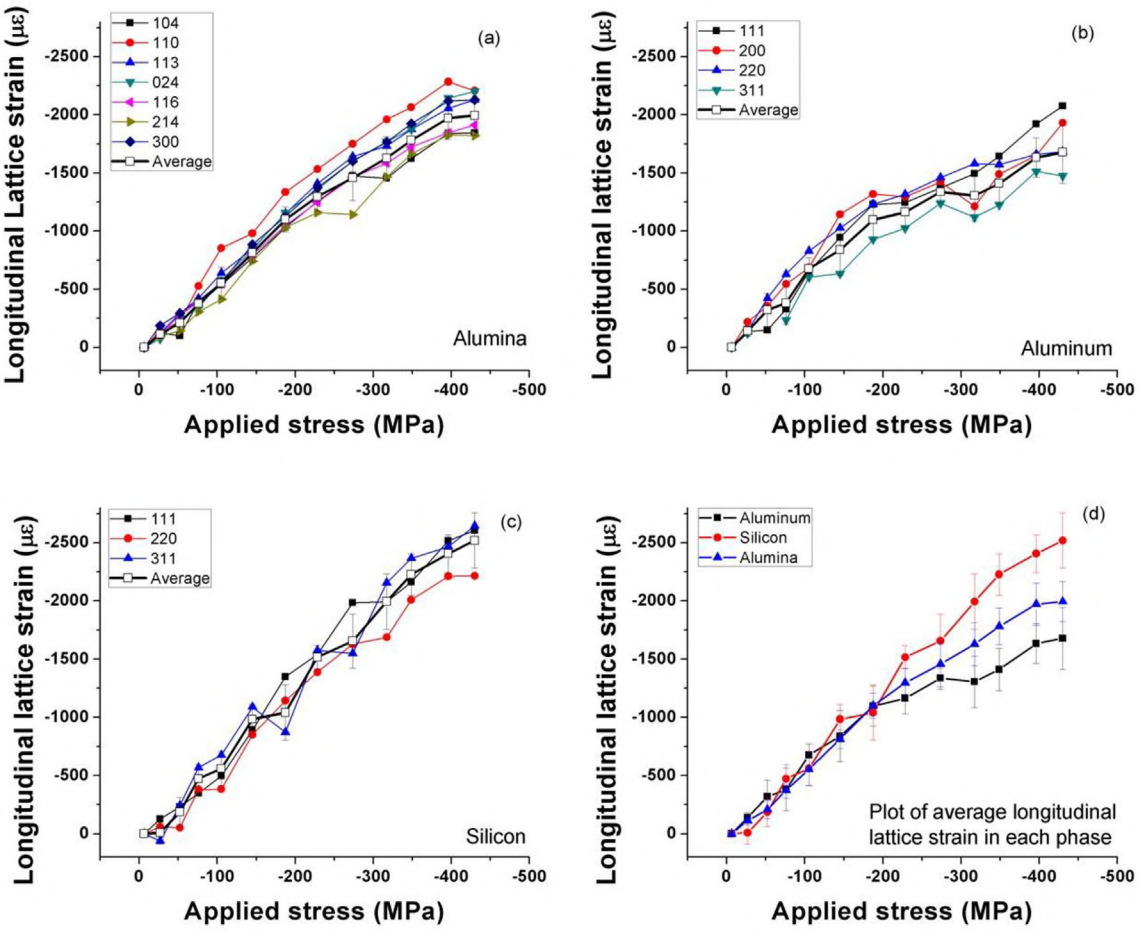

Fig. 4. Evolution of lattice strain along loading direction in all crystalline phases of the composite at different applied compressive stresses: a) alumina, (b) aluminum solid solution, (c) silicon and (d) combined plot for the average lattice strain in all three phases. (For interpretation of the references to colour in this figure legend, the reader is referred to the Web version of this article.)

remains almost unaltered until very high loading stresses. This can probably be attributed to initiation of early damage in the alumina phase (e.g. cracking of the ceramic phase or delamination at the metal/ceramic interphase) which limits its load carrying capacity even at rather low applied compressive stresses.

Diffraction line spacings measured at a ψ-tilt of 0° at different applied compressive stresses were used to determine the lattice strain in all indexed diffraction planes at a direction transverse to the direction of applied compressive stress. Here onwards, the strain so determined will be termed as transverse lattice microstrain. Fig. 5 shows the evolution of the continuum mechanics average transverse lattice microstrain in all three phases as a function of the applied compressive stress. The figure clearly shows the different trend shown by aluminum phase in comparison to both alumina and silicon. As lattice strain is being measured along transverse direction, due to the positive Poisson's ratio, transverse strain should be positive in all three phases. The plot shows that it is indeed so for silicon and alumina. However, over the course of the applied compressive stress range the aluminum solid solution phase displays a transition in behaviour. Until about 100 MPa compressive stress, the lattice strain in aluminum is also positive, as expected due to elastic deformation at this stage. However, at higher applied stresses, corresponding to its plastic deformation, the transverse lattice strains in aluminum solid solution become negative. Similar behavior was also reported in earlier studies [23,27] and it can be attributed to a change in Poisson's ratio of aluminum from about 0.35 in the region of elastic deformation to 0.5 in the region of plastic deformation. As the Poisson's ratio suddenly increases, aluminum solid solution tries to undergo an

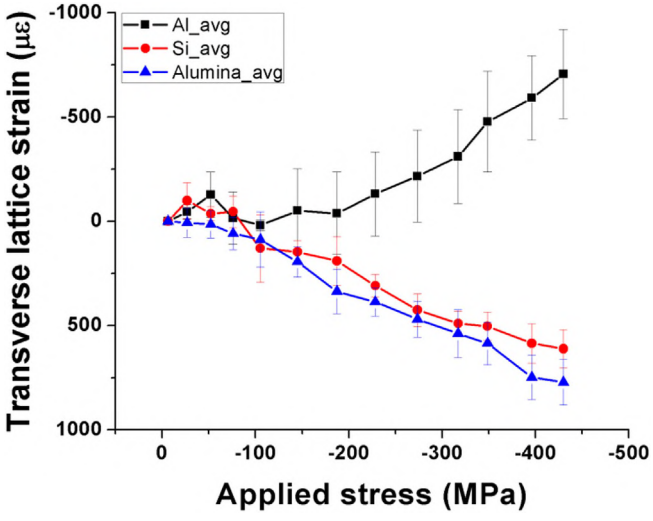

Fig. 5. Evolution of continuum mechanics average transverse lattice microstrain in all three phases of the composite as a function of applied compressive stress.

increased transverse strain, which is however constricted by the much stiffer and stronger alumina and silicon phases and the presence of strong interfacial bonding. Correspondingly, the effective transverse strain in the highly constricted aluminum solid solution becomes

compressive in nature in the region of plastic deformation. Additionally, the observed slope change at 100 MPa compressive stress further corroborates the fact that the inception of plastic deformation in aluminum solid solution phase starts at this point.

Average phase stress along the loading direction (hereafter referred to as longitudinal phase stress) can be calculated according to the following relation [37] assuming each phase is macroscopically isotropic. The validity of the assumption of isotropy in the three phases concerned (alumina, aluminium solid solution and silicon) was discussed in detail in Ref. [27]. In both alumina and aluminium solid solution the elastic anisotropy is rather small and average strain was calculated from multiple diffraction planes. Silicon has a rather large anisotropy ratio and lattice strains measured from only three diffraction planes were used to calculate the average strain. Correspondingly, for silicon, the assumption of isotropy may cause some errors in stress calculation.

$$\sigma_1 = \frac{E}{1+\nu}\cdot\varepsilon_1 + \frac{\nu\cdot E}{(1+\nu)\cdot(1-2\nu)}\cdot(\varepsilon_1+\varepsilon_2+\varepsilon_3) \quad (2)$$

where σ_1 is the longitudinal phase stress, ε_1 is the average lattice strain in each phase along the loading direction, ε_2 and ε_3 are the average lattice strains in each phase along transverse direction while E and ν are respectively the Young's modulus and Poisson's ratio of each phase. The macroscopic Young's modulus and Poisson's ratio of Al, Si and alumina were used for calculation (Table 1 of [24] lists these values). Thorough analysis of the elastic properties of this composite was carried out in an earlier work [30] and the composite behaves as an isotropic material. Correspondingly, the measured lattice strain transverse to the loading direction has been taken as the resulting lattice strain along both 2 and 3 directions ($\varepsilon_2 = \varepsilon_3$).

The evolution of the longitudinal stress, calculated according to eqn. (2), in all three phases as a function of the applied stress is shown in Fig. 6. Lines for different constant ratios of the longitudinal stress to the applied stress ranging from 0.25 to 3.0 are also shown in the same figure. The plot shows that at all applied compressive stresses, the highest longitudinal stress is always observed in alumina, while it is the lowest in aluminum solid solution. This can be attributed to the significantly higher stiffness of alumina. Until about 100 MPa compressive stress, the ratio of the longitudinal stress to applied stress in alumina lies within 1.5–2.0. At higher applied stresses, this ratio for alumina increases marginally to between 2.0 and 2.5 and becomes highest at an applied compressive stress of 187 MPa. This increase in the phase stress in alumina is caused by the load transfer from the aluminum solid solution, as already discussed. At still higher applied stresses, the stress ratio for alumina continuously decreases – which can be attributed to continuous exhaustion of its load bearing capacity due to progressive damage evolution. Throughout the range of the applied compressive stress, the ratio of the longitudinal stress to applied stress in silicon remains relatively constant and close to unity, suggesting that no significant load transfer occurs within the metallic alloy phase itself from aluminum solid solution to the stiffer and stronger needle shaped silicon phase. The evolution of longitudinal stress in aluminum solid solution shows a behaviour that compliments the trend observed in alumina. Immediately following the plastic deformation at around 100 MPa compressive stress, the ratio of longitudinal stress to applied stress in aluminum solid solution decreases marginally due to load transfer from this phase. The stress ratio attains its lowest value at an applied compressive stress of 317 MPa. At even higher applied compressive stresses, as the stress ratio in alumina continuously decreases due to damage initiation, the stress ratio in aluminum solid solution shows an increase, suggesting a higher proportion of load being carried by this phase to maintain the stress balance in the composite.

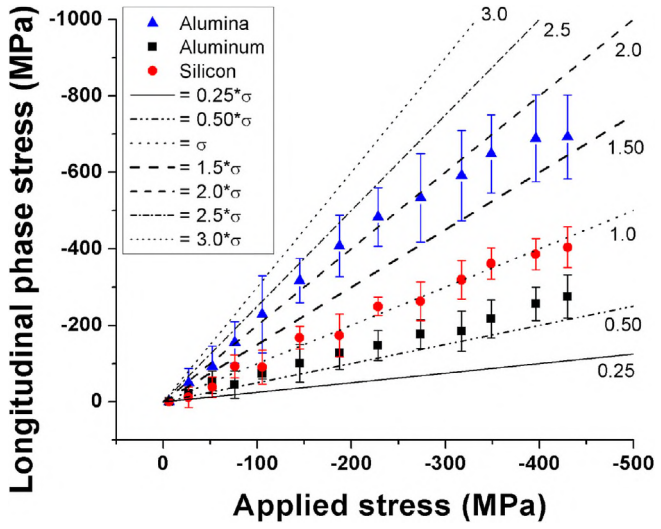

Fig. 6. Evolution of the longitudinal stress in all three phases as a function of the applied compressive stress.

4. Conclusions

The mechanism of internal load transfer in an interpenetrating metal/ceramic composite fabricated by infiltration of Al12Si melt in an open porous alumina preform was studied for the first time in this work. The preform was fabricated using a 1:1 mixture of two different polymer waxes having very different particle diameters as pore formers. It is possible to vary both the powder mixture ratios as well as the total polymer content to fabricate porous preforms as well as interpenetrating composites having different ceramic contents and pore morphologies. Study of internal load transfer in all three crystalline phases of the composite, i.e. alumina, aluminum solid solution and pure silicon was carried out using energy dispersive synchrotron x-ray diffraction. Using this technique lattice strain was measured in several diffraction planes of the three phases both along and transverse to the loading direction. The continuum mechanics average lattice strain for each phase was calculated based on the strain measured from individual diffraction planes. As lattice strains were measured from multiple diffraction planes, the reported data was more representative of the macroscopic material behaviour. Stress in each phase along the loading direction was calculated from the measured lattice microstrain and assuming isotropy of the material. Following conclusions are drawn:

a) Until about 100 MPa applied compressive stress all three phases undergo elastic deformation with lattice microstrain along the loading direction increasing with increasing applied stress at a more or less constant rate.
b) Aluminum being soft and compliant, at applied compressive stresses higher than 100 MPa, it starts deforming plastically. Consequently, its load carrying capacity decreases and more load is carried by the stiffer and stronger alumina phase. However, the increase in load carried by alumina concurrent to the plastic deformation of aluminum solid solution is not significant, as alumina itself undergoes relaxation (probably resulting from cracking or debonding) starting at a rather early stage of deformation.
c) At applied compressive stresses higher than 187 MPa the ratio of the phase stress to applied stress for alumina decreases continuously. This is concurrent with an increase in the stress ratio in aluminum solid solution to maintain stress balance. Throughout, the stress ratio in silicon remains almost constant, suggesting no significant load transfer mechanism operating within the metallic alloy itself.

Data availability statement

Raw research data used for this publication will be made available on request.

Acknowledgements

Financial support from the German Research Foundation within the Project RO4164/1-1 is gratefully acknowledged. The authors further thank TER HELL & CO. GmbH for supplying the polymer waxes used as pore formers and EDDI beamline at BESSY, Berlin for the excellent technical support during the diffraction experiment.

References

[1] M. Sternitzke, M. Knechtel, M. Hoffmann, E. Broszeit, J. Roedel, Wear properties of alumina/aluminum composites with interpenetrating networks, J. Am. Ceram. Soc. (1996) 121–128.
[2] H. Prielipp, M. Knechtel, N. Claussen, S.K. Streiffer, H. Müllejans, M. Rühle, J. Rödel, Strength and fracture toughness of aluminum/alumina composites with interpenetrating networks, Mater. Sci. Eng. A 197 (1995) 19–30, https://doi.org/10.1016/0921-5093(94)09771-2.
[3] G. Roudini, R. Tavangar, L. Weber, A. Mortensen, Influence of reinforcement contiguity on the thermal expansion of alumina particle reinforced aluminium composites, Int. J. Mater. Res. (2010) 1113–1120.
[4] R. Newnham, D. Skinner, L.E. Cross, Connectivity and piezoelectric-pyroelectric composites, Mater. Res. Bull. 13 (1978) 525–536.
[5] N. Chawla, K.K. Chawla, Metal Matrix Composites, Springer, 2013.
[6] G. Garces, G. Bruno, A. Wanner, Load transfer in short fibre reinforced metal matrix composites, Acta Mater. 55 (2007) 5389–5400, https://doi.org/10.1016/j.actamat.2007.06.003.
[7] R.J. Arsenault, L. Wang, C.R. Feng, Strengthening of composites due to microstructural changes in the matrix, Acta Metall. Mater. 39 (1991) 47–57, https://doi.org/10.1016/0956-7151(91)90327-W.
[8] K. Seol, A.D. Krawitz, J.W. Richardson, C.M. Weisbrook, Effects of WC size and amount on the thermal residual stress in WC-Ni composites, Mater. Sci. Eng. A 398 (2005) 15–21, https://doi.org/10.1016/j.msea.2005.01.041.
[9] F. Delannay, Thermal stresses and thermal expansion in MMCs, in: A. Kelly, C. Zweben (Eds.), Compr. Compos. Mater, vol. 3, 2000.
[10] S. Hong, H. Tezuka, A. Kamio, Effects of thermal residual stress on mechanical properties of SiC whisker reinforced Al-Mg and Al-Li alloys composites, Mater. Trans. JIM 37 (1996) 975–982.
[11] D. Zahl, R. Mcmeeking, The influence of residual stress on the yielding of metal matrix composites, Acta Metall. Mater. 39 (1991) 1117–1122.
[12] D.H. Bacon, L. Edwards, J.E. Moffatt, M.E. Fitzpatrick, Synchrotron X-ray diffraction measurements of internal stresses during loading of steel-based metal matrix composites reinforced with TiB2 particles, Acta Mater. 59 (2011) 3373–3383, https://doi.org/10.1016/j.actamat.2011.02.012.
[13] Y. Tomota, T. Suzuki, A. Kanie, Y. Shiota, M. Uno, A. Moriai, N. Minakawa, Y. Morii, In situ neutron diffraction of heavily drawn steel wires with ultra-high strength under tensile loading, Acta Mater. 53 (2005) 463–467, https://doi.org/10.1016/j.actamat.2004.10.003.
[14] B. Clausen, M.A.M. Bourke, D.W. Brown, E. Üstündag, Load sharing in tungsten fiber reinforced Kanthal composites, Mater. Sci. Eng. A 421 (2006) 9–14, https://doi.org/10.1016/j.msea.2005.10.004.
[15] G. Requena, G. Garcés, M. Rodríguez, T. Pirling, P. Cloetens, 3D architecture and load partition in eutectic Al-Si alloys, Adv. Eng. Mater. 11 (2009) 1007–1014, https://doi.org/10.1002/adem.200900218.
[16] M.L. Young, R. Rao, J.D. Almer, D.R. Haeffner, J.A. Lewis, D.C. Dunand, Load partitioning in Al2O3-Al composites with three-dimensional periodic architecture, Acta Mater. 57 (2009) 2362–2375, https://doi.org/10.1016/j.actamat.2009.01.019.
[17] M.L. Young, R. Rao, J.D. Almer, D.R. Haeffner, J.A. Lewis, D.C. Dunand, Effect of ceramic preform geometry on load partitioning in Al2O3-Al composites with three-dimensional periodic architecture, Mater. Sci. Eng. A 526 (2009) 190–196, https://doi.org/10.1016/j.msea.2009.07.033.
[18] T.E. Wilkes, B.J. Harder, J.D. Almer, K.T. Faber, Load partitioning in honeycomb-like silicon carbide aluminum alloy composites, Acta Mater. 57 (2009) 6234–6242, https://doi.org/10.1016/j.actamat.2009.08.050.
[19] Y.C. Hung, J.A. Bennett, F.A. Garcia-Pastor, M. Di Michiel, J.Y. Buffière, T.J.A. Doel, P. Bowen, P.J. Withers, Fatigue crack growth and load redistribution in Ti/SiC composites observed in situ, Acta Mater. 57 (2009) 590–599, https://doi.org/10.1016/j.actamat.2008.09.042.
[20] C. Yu, Z. Liu, Y. Liu, Y. Shao, Y. Ren, L. Cui, Load transfer in phase transforming matrix-nanowire composite revealing the significant load carrying capacity of the nanowires, Mater. Des. 89 (2016) 721–726, https://doi.org/10.1016/j.matdes.2015.10.029.
[21] J. Zhang, Y. Liu, Y. Ren, Y. Huan, S. Hao, C. Yu, Y. Shao, Y. Ru, D. Jiang, L. Cui, In situ synchrotron X-ray diffraction study of deformation behavior and load transfer in a Ti2Ni-NiTi composite, Appl. Phys. Lett. 105 (2014), https://doi.org/10.1063/1.4892352.
[22] M. Meixner, M.E. Fitzpatrick, W. Reimers, Measurement of the evolution of internal strain and load partitioning in magnesium hybrid composites under compression load using in-situ synchrotron X-ray diffraction analysis, Compos. Sci. Technol. 71 (2011) 167–176, https://doi.org/10.1016/j.compscitech.2010.11.003.
[23] S. Roy, J. Gibmeier, A. Wanner, In situ study of Internal load transfer in a novel metal/ceramic composite exhibiting lamellar microstructure using Energy dispersive synchrotron X-ray diffraction, Adv. Eng. Mater. 11 (2009), https://doi.org/10.1002/adem.200800352.
[24] S. Roy, J. Gibmeier, V. Kostov, K.A. Weidenmann, A. Nagel, A. Wanner, Internal load transfer and damage evolution in a 3D interpenetrating metal/ceramic composite, Mater. Sci. Eng. A 551 (2012), https://doi.org/10.1016/j.msea.2012.05.016.
[25] Y. Sinchuk, S. Roy, J. Gibmeier, R. Piat, A. Wanner, Numerical study of internal load transfer in metal/ceramic composites based on freeze-cast ceramic preforms and experimental validation, Mater. Sci. Eng. A 585 (2013) 10–16, https://doi.org/10.1016/j.msea.2013.07.022.
[26] S. Roy, J. Gibmeier, V. Kostov, K.A. Weidenmann, A. Nagel, A. Wanner, Load Partitioning Study in a 3D Interpenetrating AlSi12/Al2O3 Metal/ceramic Composite, (2014), https://doi.org/10.4028/www.scientific.net/MSF.772.103.
[27] S. Roy, J. Gibmeier, V. Kostov, K.A.A. Weidenmann, A. Nagel, A. Wanner, Internal load transfer in a metal matrix composite with a three-dimensional interpenetrating structure, Acta Mater. 59 (2011) 1424–1435, https://doi.org/10.1016/j.actamat.2010.11.004.
[28] A. Pyzalla, B. Reetz, A. Jacques, J. Feiereisen, O. Ferry, T. Buslaps, W. Reimers, In-situ investigation of strain relaxation in an Al/Si-MMC using high energy synchrotron radiation, Zeitschrift Fuer Met 95 (2004) 624–630.
[29] M.E. Fitzpatrick, A. Lodini, Analysis of Residual Stress by Diffraction Using Neutron and Synchrotron Radiation, Taylor & Francis, 2003.
[30] S. Roy, K.G. Schell, E.C. Bucharsky, K.A. Weidenmann, A. Wanner, M.J. Hoffmann, Processing and characterization of elastic and thermal expansion behaviour of interpenetrating Al12Si/alumina composites, Mater. Sci. Eng. A 743 (2019) 339–348, https://doi.org/10.1016/j.msea.2018.11.100.
[31] Y. Sinchuk, S. Roy, J. Gibmeier, R. Piat, A. Wanner, Numerical study of internal load transfer in metal/ceramic composites based on freeze-cast ceramic preforms and experimental validation, Mater. Sci. Eng. A 585 (2013), https://doi.org/10.1016/j.msea.2013.07.022.
[32] J. Davies, ASM Specialty Handbook on Aluminum and Aluminum Alloys, ASM International, 1996.
[33] S. Ahmad, J. Hashim, M. Ghazali, The effects of porosity on mechanical properties of cast discontinuous reinforced metal-matrix composite, J. Compos. Mater. 39 (2005) 451–466.
[34] C. Genzel, I. Denks, J. Gibmeier, M. Klaus, G. Wagener, The materials science synchrotron beamline EDDI for energy-dispersive diffraction analysis, Nucl. Instrum. Methods Phys. Res. Sect. A 578 (2007) 23–33.
[35] E. Macherauch, P. Mueller, Das sin2y-Verfahren der roentgenographischen Spannungsmessung, Zeitschrift Fuer Angew. Phys. 13 (1961) 305.
[36] M. Daymond, The determination of a continuum mechanics equivalent elastic strain from the analysis of multiple diffraction peaks, J. Appl. Phys. 96 (2004) 4263–4272.
[37] G. Dieter, Mechanical Metallurgy - Dieter. George Ellwood.Pdf, (1961), pp. 370–371.